*sustainability*

MDPI

*Article*

# A Sustainable Optimization Framework for Demand-Side Energy Scheduling in Grid-Connected Microgrid Management System

**Kayode Ebenezer Ojo [1], Akshay Kumar Saha [1,*] and Viranjay M. Srivastava [1,2]**

[1] Discipline of Electrical, Electronic and Computer Engineering, University of KwaZulu-Natal, Durban 4041, South Africa; ojok@ukzn.ac.za (K.E.O.); viranjay@ieee.org (V.M.S.)
[2] Department of Electronics Engineering, Birmingham City University, Birmingham B4 7XG, UK
* Correspondence: saha@ukzn.ac.za

**Abstract**

The growing integration of renewable energy sources in grid-connected microgrids (MG) has made it increasingly challenging to attain the most cost-effective and emission-efficient power dispatch in the face of uncertainty. This study addresses the scheduling problem of MG under utility-induced demand side load participation level for residential areas. Our research overcomes the constraints of conventional techniques by utilizing quantum-inspired particle swarm optimization (QPSO) to improve the operational efficiency and resilience of MG's. In this study, a three-stage stochastic framework is proposed to address the optimal energy scheduling of MGs while taking economic and emission aspects into account. Using real-time meteorological data, five Cases were investigated and simulated using MATLAB/Simulink. Without the involvement of load participation, MG's producing units in first Case, had carbon emissions of 797.110 kg and an operating cost of 267.10 €. Similar to this, the impact of demand side on the MG was evaluated in the remaining Cases. According to the simulation results, the fifth Case, which has optimal DGs scheduling, is the suggested way to improve MGs efficiency and provide a dependable power supply with low operating costs, emission reduction, and convergence features. This study not only demonstrates the practicality of QPSO algorithms but also paves the way for more resilient, efficient, and sustainable energy systems.

**Keywords:** grid-connected microgrid; demand side; load management; quantum-inspired; particle swarm optimization; sustainable energy systems

## 1. Introduction

The installation and integration of renewable energy-based microgrids (MGs) into electrical power systems promote sustainable development, increase energy supply diversity, and enable meeting the climate change targets that most nations have set [1]. As defined by the US Department of Energy (DOE) [2], MGs are small, self-sufficient power networks that may function independently of the main grid and use local energy sources to improve sustainability and energy security [3]. On the other hand, MGs have drawn a lot of interest because of their adaptability and effectiveness in combining various renewable energy sources (RESs) to satisfy regional energy needs. These systems offer greater energy security because they can function in both grid-connected and islanded modes [4]. Through the integration of numerous dispersed energy sources, including energy storage devices, wind turbines, and solar panels, MGs may adjust to changing energy needs while lowering their reliance on conventional fossil fuels. In remote areas, MGs are essential for improving

Check for updates

Academic Editor: Abdul-Sattar Nizami

Received: 20 October 2025
Revised: 26 January 2026
Accepted: 10 February 2026
Published: 12 March 2026

**Copyright:** © 2026 by the authors. Licensee MDPI, Basel, Switzerland. This article is an open access article distributed under the terms and conditions of the Creative Commons Attribution (CC BY) license.

energy accessibility, sustainability, and resilience [5]. By supporting reactive power, MGs improve voltage stability, lower greenhouse gas emissions, and offer decentralized power generation. Furthermore, MGs improve demand responsiveness, enhance energy supply reliability, and reduce transmission losses. Although MGs have many advantages, they also have drawbacks, including the high unpredictability and variability of RESs, the challenge of supply and demand matching, and limited microgrid scalability. These difficulties have prompted targeted studies on microgrid energy management systems (EMS) [6,7]. EMS is an essential component of microgrid operations since it makes it possible to optimize the balance between power supply and demand. The authors of Ref. [8] provide a thorough overview of current advancements in energy management techniques for MG, including heuristic, intelligent, and classical algorithms. Additionally, it covers important applications for energy management, such as control structure, data management, demand response, and forecasting. The article also provides an outlook on new fields of study and research areas that could improve energy management techniques. In order to guarantee that power is delivered at the lowest feasible operating cost, EMS coordinates generating and distribution activities, providing crucial functionality as a control system [9,10]. The energy management of MG's grid-connected and islanded modes varies according to operational requirements. EMS's main goal in the grid-connected mode is to maximize profits based on market prices and DG bidding costs; in the islanded mode of operation, the focus is on optimizing customer satisfaction to ensure a steady supply to the important loads [11].

Furthermore, seasonal variations in demand and the intermittent and stochastic nature of renewable energy sources (RESs) present serious operational challenges that call for advanced optimization techniques to guarantee effective operation scheduling under a range of loading conditions and objectives. These difficulties include preserving the energy balance, cutting expenses, making the most of renewable resources, and guaranteeing system dependability in a range of environmental circumstances. To address these challenges, this research uses a probabilistic approach to create the microgrid management system (MGMS) problem. The objective is to achieve optimal energy scheduling while reducing operating costs. For microgrid energy management systems to schedule optimally, demand-side management (DSM) is essential. Microgrids may actively control and alter end users' electricity consumption profiles by incorporating DSM methods, which enhances system flexibility and efficiency. Energy consumption patterns can be influenced, and effective non-critical load control can be made possible by integrating DSM programs into the MGMS problem. This integration improves the microgrid's overall operational economy and reliability by enabling a coordinated adjustment of controlled loads, distributed generation (DG), and energy storage systems (ESS) [12,13]. In particular, DSM makes it possible to shift or reduce non-critical loads during peak periods, which lowers operating costs, eases network congestion, and increases the use of renewable energy sources. By matching load demand with the availability of renewable generation sources like photovoltaic (PV) and wind power, it also helps reduce reliance on high-emission or expensive generation units. Additionally, by balancing supply-demand fluctuations, DSM helps maintain grid stability, which is crucial in microgrids that are isolated or have weak grid connections [14]. There are several ways to include DSM into the scheduling system, such as load prioritizing techniques, incentive-based demand response, and real-time pricing. By encouraging customers to take part in system optimization, these techniques turn them from passive users into active participants in energy sustainability. DSM is therefore an essential part of intelligent energy management systems since it improves microgrids' economic and environmental performance [15].

In order to reduce utility power trading prices and microgrid operation costs, this study looks at various percentages of DSM involvement by residential loads. Conventional techniques for improving residential microgrid operations frequently depend on heuristic or deterministic algorithms, which are unable to manage the high-dimensional, combinatorial nature of energy scheduling decisions, especially when there are several uncertainties present [16]. The demand for sophisticated computational methods that can manage intricate, real-time optimization is growing as MGs move toward more demand-side and intelligent energy systems. The authors of Ref. [17] investigate the application of sophisticated machine learning methods, particularly Support Vector Regression (SVR), to improve the effectiveness and dependability of power scheduling in grid-connected microgrids with numerous dispersed energy resources. In order to precisely schedule the power generation, the study's suggested SVR algorithm makes use of extensive historical energy production data, precise weather patterns, and dynamic grid circumstances. When compared to conventional linear regression models, the model showed considerably lower error metrics. Its success in increasing energy management efficiency is demonstrated by the improved prediction accuracy, which directly leads to optimum resource allocation, allowing for more accurate control of energy generation schedules and lowering total operating costs.

Within this framework, new developments in quantum-inspired computing present viable approaches to high-dimensional optimization problems related to demand-side energy scheduling. These new techniques make it possible to manage microgrid systems more effectively, balancing cost, energy consumption, and sustainability goals more quickly and precisely than with traditional techniques [18]. Combining swarm intelligence and quantum-inspired concepts, quantum particle swarm optimization (QPSO) allows for more thorough solution space search and effective multi-objective optimization. Its dynamic swarm behavior and quantum-inspired operators help it overcome common problems that classical algorithms have, like managing complex, multi-modal, and non-linear objective functions. By utilizing special qualities, such as quick convergence, resistance to local optima, and better management of multi-objective functions, which are frequently observed in conventional approaches, this clever strategy avoids premature convergence and stagnation. Likewise, the multi-objective function optimizes two or more goals at the same time, which are frequently incompatible. This results in a collection of "Pareto-optimal solutions" that represent different trade-offs rather than a single optimal solution. A more comprehensive understanding of trade-offs for complicated issues where several conflicting objectives need to be balanced is offered by multi-objective optimization. QPSO provides a practical method for energy management in MGs by optimizing DG setup to limit emissions and save operating costs. Its quantum-inspired algorithms are especially well-suited for multi-objective optimization because they balance exploration and exploitation while enabling effective exploration of intricate solution spaces. QPSO provides an unparalleled ability to investigate many solution spaces at once by utilizing quantum superposition and entanglement, greatly accelerating the convergence toward near-optimal energy dispatch techniques [19–21].

A novel QPSO-based optimization framework for resource allocation in grid-connected MGs is presented in this paper. It is intended to manage the dynamic interaction of demand-side flexibility, storage utilization, and distributed generation while guaranteeing decarbonization, cost-effectiveness, and reliability. In addition, the ability of the suggested QPSO framework to handle the two problems of economic and environmental scheduling in microgrid management is demonstrated. The following summarizes the study's contributions:

- Develop a microgrid scheduling issue that incorporates important operational constraints, including power balancing, storage utilization, and grid interaction, while guaranteeing smooth compliance with quantum variational approaches.
- Presents a multi-objective framework for allocating residential MG resources that strikes a balance in terms of both computational efficiency and economic viability.
- Utilizing quantum-inspired PSO algorithms to maximize power export to the utility while determining the optimal power dispatch configuration for DG resources.
- Demonstrates the superiority of the QPSO-based scheduling framework through the incorporation of demand side load participation levels and the utilization of real-time weather data.

## 2. Review of Several Techniques

Conventional microgrid optimization techniques have mostly focused on deterministic methods, such as mixed-integer linear programming (MILP) and mixed-integer nonlinear programming (MINLP), which explicitly represent cost functions, operational constraints, and power flow equations. They have been widely used to address storage management, generation scheduling, and economic dispatch issues [22,23]. Deterministic models offer mathematically sound solutions, but they have scalability problems, especially when it comes to the high-dimensional optimization environment of microgrids with many DERs and dynamic constraints. Furthermore, accurate forecasting of renewable generation and load demand is frequently necessary for deterministic models, which are intrinsically uncertain [24,25]. Consequently, stochastic optimization has been implemented to take into consideration fluctuations in the supply and demand for energy. By including probabilistic constraints and uncertainty distributions, stochastic programming techniques like scenario-based approaches and chance-constrained optimization have become more robust [26]. However, these approaches are not feasible for real-time microgrid operations due to their substantial rise in computational cost, which occurs when the number of scenarios increases exponentially with the problem size [10].

For microgrid optimal scheduling, metaheuristic algorithms, including genetic algorithms (GA), particle swarm optimization (PSO), and simulated annealing (SA), have become popular because they work well for traversing vast search spaces and reduce the computational load of deterministic and stochastic techniques. These nature-inspired optimization methods require fewer assumptions about the issue structure and offer flexibility in solving complicated, nonlinear, and multi-objective problems [27]. For instance, PSO has been successfully used to maximize DER dispatch by iteratively improving swarm intelligence-based solutions, and GA has been shown to be useful in maximizing microgrid resilience in the face of severe weather. Notwithstanding their benefits, metaheuristic approaches have limitations in their application for large-scale microgrid scheduling challenges due to their difficulties with convergence and the need for substantial parameter adjustment. Additionally, these algorithms frequently perform less than optimally since they are unable to find globally ideal solutions, especially in situations with very limited energy resources [28,29].

In recent years, deep learning (DL) and reinforcement learning (RL) techniques have become popular in microgrid energy scheduling optimization, taking advantage of artificial intelligence's (AI) capacity to extract intricate patterns from data and adjust to shifting conditions. Specifically, deep reinforcement learning (DRL) has been investigated for real-time energy trading, optimal control of storage systems, and demand response management. Adaptive energy scheduling systems that dynamically adapt to variations in distributed generation (DG) have been developed using techniques like Proximal Policy Optimization (PPO) and Deep Q-Networks (DQNs). Although DRL provides a data-driven method for optimization, real-time application in microgrids is severely hampered by its dependency on sizable training datasets and substantial processing resources. Furthermore, in critical power system applications, the black-box aspect of neural networks poses questions about interpretability and reliability [30–32]. Due to the drawbacks of both classical and AI-driven approaches, quantum computing has become a viable solution for energy systems' high-dimensional optimization issues. Quantum computing processes information in ways that traditional computers cannot effectively duplicate by utilizing quantum mechanical concepts like superposition, entanglement, and interference [33].

Among the many quantum algorithms, QPSO has drawn a lot of interest for its ability to solve combinatorial optimization issues, such as logistics, energy scheduling, and portfolio optimization. The use of QPSO in energy optimization has been the subject of several studies, mainly in grid operation and power system planning [34]. In Ref. [35], a multi-stage paradigm for optimizing energy management for MGs under uncertainty, combining demand-side response (DSR) with carbon trading, was presented. The methodology utilizes the QPSO algorithm to derive optimal scheduling solutions and applies scenario analysis to handle the fluctuation of renewable energy. According to the results, using carbon trading lowers emissions and the consumption of fossil fuels, while increased DSR participation boosts microgrid economic performance by as much as 27.48%. Similarly, in order to lower operating costs and environmental emissions, the authors [36] propose a multi-objective optimization framework for grid-connected microgrids that makes use of quantum particle swarm optimization (QPSO). The QPSO algorithm successfully gets beyond the drawbacks of conventional techniques by combining battery storage with both conventional and renewable energy sources. Simulation results demonstrate that QPSO achieves a 9.67% reduction in operational costs, equating to savings of €158.87, and a 13.23% reduction in carbon emissions, lowering emissions to 513.70 kg of CO2 equivalent in the economic scheduling scenario. The findings of the simulation show significant advancements, reducing costs and emissions while increasing the overall sustainability and efficiency of the microgrid. Researchers have shown that QPSO may effectively improve renewable energy forecasting, optimize transmission network expansion, and resolve unit commitment issues. QPSO is a promising tool for improving sustainable energy practices in microgrids because of its capacity to precisely explore complex optimization landscapes. Its use in demand-side management and microgrid scheduling, however, is still mostly unexplored [37].

## 3. Problem Formulation

This section explains the problem formulation and elaborates on the specific constraints, including demand-side flexibility, energy balancing, energy storage, decarbonization, and voltage stability. The primary goal of the MG optimization taken into consideration in this study is to identify the DG units' most efficient power-generating operating points within a specified timeframe. This optimization seeks to reduce operating costs as well as the quantity of emissions generated concurrently. The precise formulation of the multi-objective function would be the first step in the grid-connected MG problem's optimal energy scheduling. The next step would be the restrictions on how DG units connected to the grid might operate.

### 3.1. Objective Function

In practical microgrid scheduling, minimizing the total operational cost is a complex task requiring consideration of multiple dynamic factors. The multi-objective optimization methodology proposed in this study considers both the minimal optimization target for carbon emissions under the carbon trading market connected to the MG system, as well as the MG minimum operational cost.

https://doi.org/10.3390/su18062763

$$MinF(\chi)= f_1(\chi) + f_2(\chi) \tag{1}$$

This formulation integrates energy operational costs $f_1(\chi)$ which encompasses the cost of running each DG as well as the power interaction between the utility and MG. The price of cleaning up the gas that is created by conventional power generation techniques (environmental cost) $f_2(\chi)$.

$$\begin{gathered} f_1(\chi) = \sum_{t=1}^{T}\Big\{\sum_{i=1}^{N_{DG}} u^i(t)P_{DG}^i(t)B_{DG}^i(t) + S_{DG}^i\big(u^i(t) - u^i(t-1)\big)+ \\ \sum_{j=1}^{N_{BESS}}\Big[u^j(t)P_{BESS}^j(t)B_{BESS}^j(t) + S_{BESS}^j\big(u^j(t) - u^j(t-1)\big)\Big] + P_{grid}^t(t)B_{grid}^t(t)\Big\} \end{gathered} \tag{2}$$

Vector $\chi$ represent the important active power decision variables, $i^{th}$ of DG units, and $j^{th}$ of BESS units in related to their switching (ON/OFF) states in a microgrid. The variables $N_{DG}$, and $N_{BESS}$ represents the overall number of DG, and BESS units connected to the MG network. The bid costs of DG, and BESS units, and utility at the hours of time 't' are denoted as $B_{DG}^i(t)$, $B_{BESS}^k(t)$, and $B_{grid}^t(t)$ respectively. While $P_{DG}^i(t)$, $P_{BESS}^j(t)$, $P_{grid}^t(t)$ are the exchanged active electricity pricing for the utility, BESS, and DG sources.

$$f_2(\chi) = \sum_{t=1}^{T}\left(\begin{array}{c} \sum_{p}^{N_{MT}} C_{carbon}(t)\Big(m_{carbon}^p(t) - C_{quota}(t)\Big) \\ +\sum_{q}^{N_{FC}} C_{carbon}(t)\Big(m_{carbon}^q(t) - C_{quota}(t)\Big) \end{array}\right) \tag{3}$$

where, $C_{carbon}(t)$ is the carbon trading market's current price, $m_{carbon}^p(t)$, and $m_{carbon}^q(t)$ denotes the microgrid's carbon emissions $C_{quota}(t)$ is the quantity of carbon allowances decided by the loads [38,39].

### *3.2. Operational Constraints*

In this study, a constraint optimization problem must be solved to manage an MG for optimal functioning. The power balancing constraint is the main obstacle to resolving the MGMS energy scheduling problem. For every time interval, the utility, BESS, and DGs' combined output power must be sufficient to meet the MG's entire load demand. Assuming that the actual power loss in the MG is disregarded.

#### 3.2.1. Power Balance Constraint

In order to guarantee steady system performance, power balance must be maintained during microgrid operation. For the energy scheduling of MG to operate steadily, one of the essential constraints is the power balancing constraint. It demands that the active power produced by DG sources, BESS, and the utility be equal to the system load demand.

$$\sum_{t=1}^{T} P_{load}(t)= \sum_{t=1}^{T}\Big(\sum_{i=1}^{N_{DG}} P_{DG}^i(t) + \sum_{j=1}^{N_{BESS}} P_{BESS}^j(t) + P_{grid}^t(t)\Big) \tag{4}$$

#### 3.2.2. Constraint of Active Power Generation

In order to ensure system security and stability, each DG unit's active power output and the power transferred between the utility and the MG are limited to predefined minimum and maximum values. These constraints on all active power generation within the ranges that are allowed are stated as follows:

$$\left.\begin{array}{c} P_{DG,min}^i \le P_{DG}^i(t) \le P_{DG,max}^i \\ P_{BESS,min}^j \le P_{BESS}^j(t) \le P_{BESS,max}^j \\ P_{grid,min}^t \le P_{grid}^t \le P_{grid,max}^t \end{array}\right\} \tag{5}$$

Strict adherence to grid limits is necessary to avoid overloading. This limitation makes sure that the net imported energy after deducting demand and the difference between discharged and charged storage power stay under the grid's maximum permitted power exchange limit, $P^t_{grid,max}$. The $P^i_{DG,min}$ and $P^i_{DG,max}$, $P^k_{BESS,min}$ and $P^k_{BESS,max}$, and $P^t_{grid,min}$ and $P^t_{grid,max}$ denotes the minimum and maximum active power outputs for each scheduling period of MG management system. The dependent variable needs to be included as a quadratic penalty term in the objective function, but the control variables are self-constrained. By enforcing penalties for deviations from ideal energy balancing, this quadratic penalty function discourages wasteful resource allocation and encourages optimal scheduling. This term adds a penalty factor called '$\lambda_{pen}$' to the objective function, which is the square of the difference between the dependent variable's actual value and its limiting value. Any impractical solution found throughout the optimization process is disregarded [40]. Additionally, the new variable $P^t_{DG,lim}$ is created, it defines the operational boundary of each DG within the microgrid optimization or scheduling model. $P^t_{grid}$ is regarded as a dependent variable to impose the power balancing constraint. The following is the expression for the newly expanded objective function that needs to be minimized:

$$MinF(\chi) = \left(f_1(\chi) + f_2(\chi)\right) + \lambda_{pen}\left(P^t_{grid} - P^t_{DG,lim}\right)^2 \tag{6}$$

#### 3.2.3. Constraint of Energy Storage System

Operations of energy storage systems are limited by their individual charge and discharge restrictions, guaranteeing that storage cannot charge and discharge at the same time. The state of charge and the limitation placed on the battery storage unit's charging/discharging pace are represented as follows in Equations (7) and (8).

$$W_{BESS,t} = W_{BESS,t-1} + \eta_{ch} P_{ch} \Delta t - \frac{1}{\eta_{dch}} P_{dch} \Delta t \tag{7}$$

$$\left.\begin{array}{c} W_{BESS,min} \leq W_{BESS,t} \leq W_{BESS,max} \\ P_{ch,t} \leq P_{ch,max};\ P_{dch,t} \leq P_{dch,max} \end{array}\right\} \tag{8}$$

where, $W_{BESS,t}$ and $W_{BESS,t-1}$ are the quantity of energy stored over a period of time $t$ and $t-1$. $\eta_{ch}$ and $\eta_{dch}$ are the charge and discharge efficiency of the storage device. $P_{ch}$ and $P_{dch}$ are the allowed rates of charging and discharging at specific times $\Delta t$. While $W_{BESS,min}(W_{BESS,max})$ and $P_{ch,max}(P_{dch,max})$ are the upper limit of the charge (discharge) rate of energy storage and the minimum (maximum) limitations of energy storage.

#### 3.2.4. Constraint of Voltage Stability

Maintaining voltage stability within permissible bounds is necessary to avoid frequency deviations and interruptions in operations. When power imbalances are weighted by voltage sensitivity coefficients, the quadratic penalty function makes sure that they don't go over a reasonable deviation level. Significant supply and demand imbalances that can result in voltage breaches are discouraged by the penalty.

$$\sum_{t=1}^{T} V_{St}(t) = \sum_{t=1}^{T}\left(\varphi_i^{N_{DG}} + \zeta_j^{N_{BESS,dis}} - \delta_t^{N_{imp}} - \psi_t^{N_{dem}}\right)^2 * \gamma_t^{voltage} \leq \varepsilon^{voltage,max} \tag{9}$$

where, $N_{imp}$ and $N_{dem}$ denotes net imported energy after deducting demand, this formulation avoids operational infractions that can jeopardize the voltage stability of microgrids. $\gamma_t^{voltage}$ is the voltage sensitivity coefficient and is the voltage deviation threshold, $\varepsilon^{voltage,max}$.

#### 3.2.5. Constraint of Decarbonization

A primary goal of microgrid operations is decarbonization, which guarantees a low dependency on fossil fuel-based grid power. This limitation weighs each power flow's emission factor to quantify the net environmental impact of the flow.

$$\sum_{t=1}^{T} C_{decar}(t) = \sum_{t=1}^{T} \left( \varphi_i^{N_{DG}} * \mu_t^{green} + \zeta_j^{N_{BESS,dis}} * \mu_t^{BESS} - \delta_t^{N_{imp}} * \mu_t^{carbon} \right) \geq \eta^{carbon,min} \tag{10}$$

where, $\mu_t^{green}$ for renewables, $\mu_t^{BESS}$ for storage discharge, and $\mu_t^{carbon}$ for grid imports. To enforce sustainable energy transitions, the weighted total must be greater than a predetermined carbon-neutrality, $\eta^{carbon,min}$ criterion [16,17].

### 3.3. Demand Side Management

This study's use of the DSM technique aims to change the intended load consumption profile to bring it closer to the optimal load profile. Flexible load-shaping DSM is a crucial tactic to accomplish the day-ahead energy scheduling issue, which aims to minimize overall operating costs and reduce system peak demand. It is best to use flexible load shaping for utility-induced DSM to fully exploit the temporal independence of controlled loads. Through the adjustment of consumer energy consumption to better match the supply of locally generated renewable power, DSM in a microgrid increases operating efficiency, lowers costs, lowers carbon emissions, and improves consistency. DSM reduces electricity bills for customers and optimizes system costs for operators. Figure 1 shows how the DSM is set up to lower electricity costs and ensure dependable communication between the utility and its customers. There are two types of DSM programs: utility-induced schemes and customer-induced schemes. It is best to use flexible load shaping for utility-induced DSM to fully exploit the temporal independence of controlled loads. The load forecast data is sent to the central DSM controller, which then assesses what has to be done to achieve the required load profile. The consumer engages in the DSM program during the hourly dispatch and gets scheduling signals via a two-way communication channel [41,42].

$$Min\ F = \sum_{t=1}^{T} (\varepsilon(t) - \delta(t))^2 \tag{11}$$

$$\varepsilon(t) = \mathcal{F}(t) + \mathbb{C}(t) - \text{Å}(t) \tag{12}$$

$\varepsilon(t)$ is the planned load provided to the DSM controller, $\delta(t)$ is optimal load profile at a specific time $t$. $\mathcal{F}(t)$, $\mathbb{C}(t)$, and $\text{Å}(t)$ represent the forecasting load, connected load, and disconnected load at time $t$ interval, respectively.

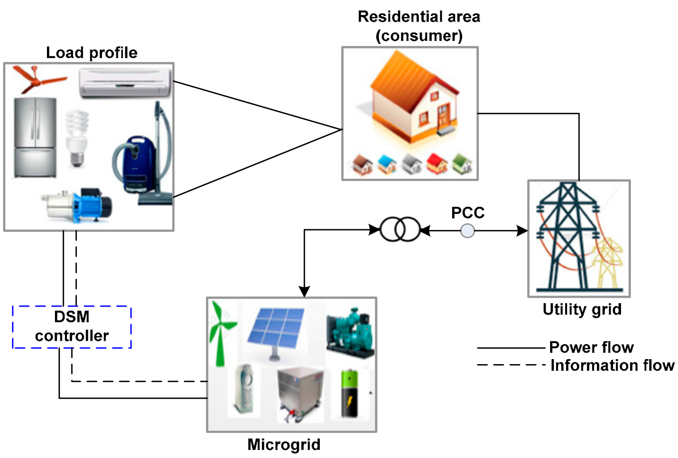


**Figure 1.** Demand side management approach [41].

By guaranteeing that a minimal percentage of demand is satisfied by storage discharge rather than external supply, Equation (13) enforces a demand-side response mechanism. The flexibility of demand shifting and storage usage is reflected in the weighting coefficients for response and storage. Before using grid electricity, the limitation ensures that distributed resources are effectively utilized.

$$Min\ F = \sum_{t=1}^{T} \left( \varphi_t^{dem} * \tau_t^{response} - \zeta_t^{BESS,dis} * \tau_t^{storage} \right) \geq \theta^{demand,shifting} \quad (13)$$

## 4. Modelling of Grid-Connected DG Units

Figure 2 shows a typical low-voltage grid-connected MG that was taken into consideration for assessing the proposed QPSO architecture [38]. The main component of this system is the MG central controller (MGCC), which is in charge of monitoring and controlling the power exchange between the utility and the MG. The primary duty of MGCC is to provide local controllers with power references to meet power balance requirements for the designated time T. Supporting this effort are the load controller (LC) and micro-source controller (MC), which are responsible for supplying or absorbing surplus (deficit) energy to meet power requirements. Energy storage devices are incorporated into this strategy to mitigate predicting risks and guarantee steady and dependable system functioning. Along with an energy storage device, the architecture incorporates several DG units, including gas-fueled microturbines (MT), fuel cells (FC), wind turbines (WT), and solar photovoltaic (PV) systems. The active power produced by all DG sources is considered to be at a unity power factor. Furthermore, the utility and the MG have a power exchange link to trade energy during the day, as determined by the MGCC's decisions.

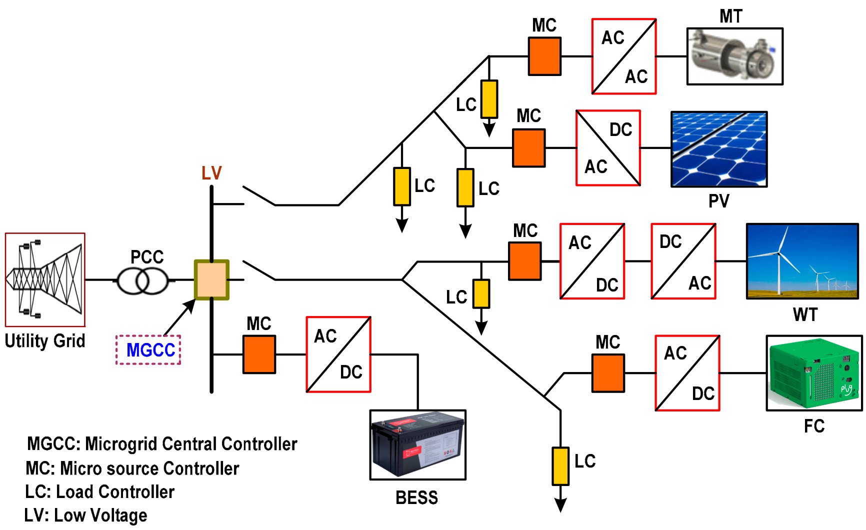


**Figure 2.** A typical low-voltage grid-connected MG system [38].

### *4.1. Solar PV Model*

The module features and metrological characteristics, such as solar irradiation $I_s$ and ambient temperature $T_a$ can affect the power output of the PV system. The following is the estimated power output $P_{PV}$ from the PV module [43]:

$$P_{PV} = P_{STC} \frac{I_s}{1000} * (1 + \alpha(T_c - 25)) \quad (14)$$

where, $P_{STC}$ stands for the maximum power (W) of the solar module under standard test conditions (STC). On the surface of the photovoltaic module, $I_s$ represents the sun irradiation $\left(\mathrm{W/m^2}\right)$. $T_c$ denotes the temperature of the photovoltaic cell (module) (°C), while

$\alpha$ represent the temperature coefficient for power ($^{\circ}C^{-1}$). The standard test settings $I_{STC}$ have a sun irradiation of 1000 kW/m$^2$. According to conventional test circumstances, $T_{STC}$ working temperature is 25 °C. The nominal operating cell temperature (NOCT) of the photovoltaic module can be used to determine the module's temperature in relation to ambient temperature and solar irradiation. This is the expression for the NOCT model equation:

$$T_c = T_a + \frac{I_s}{800} * (T_{NOCT} - 20) \quad (15)$$

where, $T_a$ denotes the ambient temperature (°C), and $T_{NOCT}$ denote the normal operating cell temperature (°C) of the module. $T_{NOCT}$ is the module's normal operating cell temperature (°C), and $T_a$ is the ambient temperature (°C). Additionally, Equation (13) estimates the likelihood of a discrete state for solar uncertainty modeling, in which $f_{PV}(\zeta)$ is used to indicate the hourly solar irradiation. $\zeta_1$, and $\zeta_2$ are the irradiance limitations represented by the random variable $(\zeta)$, $\rho(\zeta)$ is the accumulated PV-related quantity over the range $\zeta_1$, and $\zeta_2$. The variable '$\zeta$' represents the solar irradiance (W/m$^2$).

$$\rho(\zeta) = \int_{\zeta_1}^{\zeta_2} f_{PV}(\zeta) d\zeta \quad (16)$$

### *4.2. Wind Turbine Model*

The intermittent nature of the wind is the primary determinant of the power generated by a wind turbine. Two key variables, such as the wind speed at a specific location and the wind turbine's power curve, must be understood to compute the power output of a wind turbine. A wind turbine's power curve can be represented using a function that is divided into three (3) distinct portions [44]:

$$P_{WT} = \begin{cases} 0 & v \le v_{ci} \\ \frac{v^2 - v_{ci}^2}{v_{nom}^2 - v_{ci}^2} * P_{WT,nom} & v_{ci} < v \le v_{nom} \\ P_{nom} & v_{nom} < v \le v_{co} \end{cases} \quad (17)$$

where, $P_{WT,nom}$, $v_{nom}$, $v_{ci}$, and $v_{co}$ are nominal power, nominal wind speed, cut-in wind speed and cut-out wind speed, respectively. $P_{WT}$ is the power output of the wind turbine (kW), and $v$ is the wind speed (m/s). The cut-in wind speed and cut-out wind speed, are 5 m/s and 10 m/s respectively. The rated wind speed and rated nominal power are 15 m/s and 30 kW. Weibull distribution is frequently used to depict the temporal variations in wind speed. The Weibull probability distribution function can be expressed as follows:

$$f_{WT} = \begin{cases} \frac{\beta}{\gamma} * \left(\frac{v}{\gamma}\right)^{\beta-1} * e - ^{\left(\frac{v}{\gamma}\right)^{\beta}} & v \ge 0 \\ 0 & Otherwise \end{cases} \quad (18)$$

### *4.3. DG Bid Costs Calculation*

Considering the PV, WT, and BESS production cost (PC) and depreciation cost (DC), calculated at each time interval t. For an integrated system, the bid cost function for the DG unit $(B_{DG,\ cost})$ over a time horizon T can be expressed as:

$$B_{DG,\ cost} = \sum_{t=1}^{T} (PC_{PV,t} + PC_{WT,t} + PC_{BESS,t} + DC_{BESS,t}) \quad (19)$$

PV, WT, and BESS have nearly zero fuel costs. Their production costs are primarily their operation and maintenance (O&M) costs, which are often considered fixed per unit of energy generated over time.

$$PC_{PV,t}= C_{OM,PV} \times P_{PV,t} \tag{20}$$

$$PC_{WT,t}= C_{OM,WT} \times P_{WT,t} \tag{21}$$

$$PC_{BESS,t}= C_{OM,BESS} \times \left(\left|P_{BESS,charge,t}\right| + \left|P_{BESS,discharge,t}\right|\right) \tag{22}$$

where, $C_{OM,PV}$ and $C_{OM,WT}$ are the O&M cost coefficients (€/kWh) and $P_{PV,t}$ and $P_{WT,t}$ are the power outputs at time t. While $C_{OM,BESS}$ is the O&M cost coefficient for BESS (€/kWh). The overall bid cost function for the DG unit $(B_{DG})$ incorporating these elements at a specific time is expressed as:

$$B_{DG}= C_{OM,PV}P_{PV,t} + C_{OM,WT}P_{WT,t} + C_{OM,BESS}P_{BESS,t} + DC_{BESS,t} \tag{23}$$

Similarly, MT and FC bids are determined as follows:

$$B_{DG}= C_{fuel} * \frac{P_{DG}}{\eta_{DG}} + C_{inv} \tag{24}$$

$$C_{inv}= DC * \frac{P_{DGnom}}{PC} \tag{25}$$

$$DC= \frac{r(1+r)^n}{(1+r)^n - 1} * IC \tag{26}$$

where, $C_{fuel}$ is the cost of the fuel (€), $\eta_{DG}$ is the efficiency, $C_{inv}$ is the annual cost of production and depreciation investments. $P_{DGnom}$ represent the nominal DG power (kW). where, variable 'r' denotes the annual benchmark interest rate, and the cost of installing DG units is denoted as 'IC'.

### 4.4. DER Uncertainty Modeling

In order to solve the uncertainty problem of variables such as solar PV and WT power output, stochastic programming is frequently used [45]. Two (2) uncertainty factors, such as solar PV and wind turbines, are assumed in this analysis. The historical recorded dataset and stochastic planning method found in Refs. [37,38] are used to forecast these parameters. The following model represents the uncertainties in solar PV and WT power output:

$$P_{pv,t,s}= P^f_{pv,t} + \Delta P_{pv,t,s}: \ t = 1,\ldots, \ N_T; s= 1,\ldots, N_s \tag{27}$$

$$P_{WT,t,s}= P^f_{WT,t} + \Delta P_{WT,t,s}: \ t = 1,\ldots, \ N_T; s= 1,\ldots, N_s \tag{28}$$

where, $P^f_{pv,t}$, $P^f_{WT,t}$, $\Delta P_{pv,t,s}$, and $\Delta P_{WT,t,s}$ are forecasted output power of PV and WT, with their forecast errors respectively. $N_T$ and $N_s$ are time interval quantities, and scenario quantities are chosen for the uncertainty model. The uncertainty variables modeled, using a two year hourly recorded dataset, are simulated using MATLAB software. The observed data X, and the predicted data $X^*$ can be justified using mean square error (MSE), root mean square error (RMSE), and mean absolute percentage error (MAPE) as expressed as follows:

$$MSE= \frac{1}{n}\sum_{i=1}^{n}(X_i^* - X_i)^2 \tag{29}$$

$$RMSE= \sqrt{\frac{1}{n}\sum_{i=1}^{n}(X_i^* - X_i)^2} \tag{30}$$

$$MAPE= \frac{1}{n}\sum_{i=1}^{n}\left|\frac{X_i^* - X_i}{X_i}\right| \tag{31}$$

Weibull distribution and Gaussian process modeling are used to simulate solar PV and wind speed for testing and training in the prediction process. The artificial neural network (ANN) tool was successfully utilized to represent the uncertainty. The solar PV and wind turbine RMSEs are 0.162 and 0.184, respectively, according to the modeling findings shown in Figures 3 and 4.

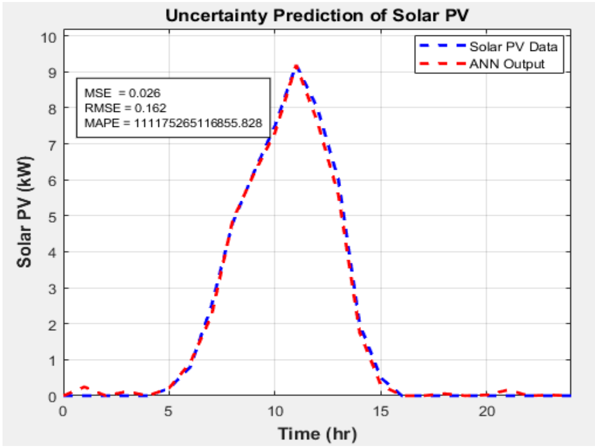


**Figure 3.** Uncertainty of solar PV prediction.

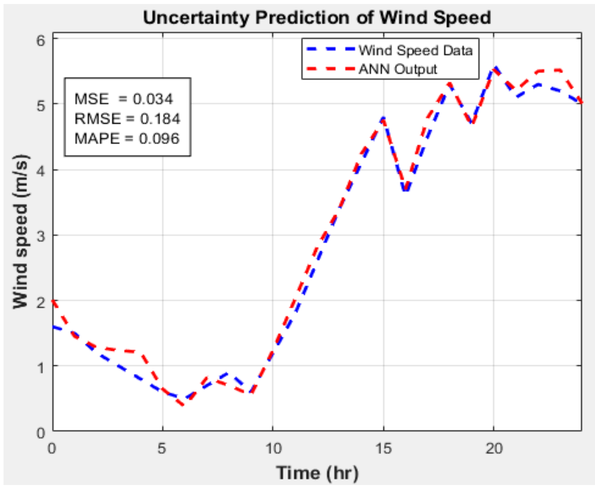


**Figure 4.** Uncertainty of wind speed prediction.

*4.5. Proposed Algorithm*

This section describes the proposed algorithm that complies with environmental constraints while achieving the best energy scheduling of MG's. One of the most well-known optimization methods that is inspired by quantum physics is QPSO. QPSO combines particle swarm optimization's (PSO) collective intelligence with ideas from quantum physics. The state transitions of PSO and QPSO is illustrated in Figure 5 [46]. The quantum rotation gate and quantum probability measurement are two examples of quantum-inspired operators that are used in QPSO to retain particle variety and explore the solution space. In order to achieve a wide range of Pareto-optimal solutions, the hybrid approach incorporated into QPSO effectively resolves multi-objective optimization problems by upholding a strong balance between exploration and exploitation. Furthermore, QPSO's capacity to actively control the search process and its flexibility in adjusting its settings make it more effective at identifying the optimum trade-off solutions for multi-objective optimization tasks [47]. In QPSO, a wave function of $\psi(\mathrm{x}, \mathrm{t})$ represents the state of a particle. The probability density function $|\psi(x,t)|^2$ can be used to calculate the possibility that the particle will exist at position $x$ in time $t$. The Equations (32) and (33) represents the normalized wave function and the associated probability density function:

$$\psi(\mathrm{x,t}) = \frac{1}{\sqrt{L}} e^{-|Y|/L} \tag{32}$$

$$|\psi(x,t)|^2 = \frac{1}{\sqrt{L}} e^{-2|Y|/L} \tag{33}$$

where, $L = h^2/m\gamma$, and $\gamma$ is in the interval [0, 1]. $\psi$ represents the wave function, $Y$ is a moving frame or spatial displacement, and $L$ represents the decay constant. When a quantum state collapses into a classical state, a Monte Carlo random simulation can be used to determine the particle's exact location. According to Equations (34) and (35), the particle's position is updated at each iteration.

$$x_{p,q}(t+1) = P_{p,q}(t) \pm \xi * \left| mbest_{p,q}(t) - x_{p,q}(t) \right| * In\left(\frac{1}{u}\right) \tag{34}$$

$$P_{p,q}(t) = \left(\varphi * P_{p,q}(t) + (1-\varphi) G_q(t)\right) \tag{35}$$

$$\varphi = \frac{c_1 r_1}{c_1 r_1 + c_2 r_2} \tag{36}$$

Provided, $(1 \le p \le N)$ and $(1 \le q \le M)$.

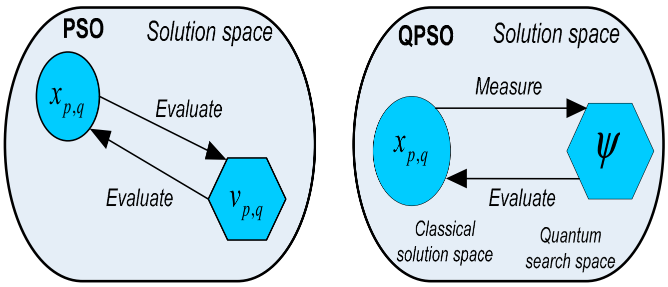


**Figure 5.** Transition state of PSO and QPSO algorithms [46].

As illustrated in Algorithm 1, QPSO integrates the idea of quantum behavior and explains how particles with quantum bound states aggregate in quantum space. In M iterations, every particle with a dimension of D out of N particles converges to its local attractor $P = P_1, P_2, P_3, \ldots, P_D$. The weighting factor, often called a sharing coefficient used to distribute or proportionally allocate quantities between two components or sources is represented as $\varphi$. The acceleration coefficients are $c_1$ and $c_2$, the randomly distributed, regularly distributed integers within [0, 1] are $r_1$, $r_2$ and $u$, respectively. The personal best and global best positions of the $p^{th}$ particle in the $q^{th}$ iteration is indicated by $P_{p,q}$ and $G_q$. For each iteration, the average of the individual best locations $mbest_{p,q}(t)$ is needed to update the lagged particles into the population.

$$mbest_{p,q}(t) = \frac{1}{N}\sum\nolimits_{p=0,q=1}^{N,M} P_{p,q}(t) = \left(\frac{1}{N}\sum\nolimits_{p=0}^{N} P_{p,1}(t), \frac{1}{N}\sum\nolimits_{p=0}^{N} P_{p,2}(t), \ldots, \frac{1}{N}\sum\nolimits_{p=0}^{N} P_{p,D}(t)\right) \tag{37}$$

The contraction–expansion coefficient, or parameter $\xi$, is defined as $\xi = 1 - (1.0 - 0.5) * k/G_m$ in the context of quantum mechanics. $k$ represents the current iteration count and $G_m$ represents the maximum number of iterations, plays a critical role in controlling the exploration and exploitation balance in the optimization process. Its selection is motivated by several considerations: In Ref. [35], the authors demonstrated that, the linearly decreasing contraction–expansion coefficients improve convergence by allowing broad exploration in the early iterations ($\xi \approx 1$) and finer local exploitation in later iterations

($\xi \approx 0.5$). Throughout the iterations, the contraction–expansion coefficient $\xi$ falls linearly from 1.0 to 0.5. Quantum-behaved particle swarm optimization and related metaheuristics have made extensive use of this approach. The contraction-expansion coefficient can be used in sensitivity analysis to examine how various schedules affect the rate of convergence and the quality of the solution. The performance on benchmark tasks with an effective range of 0.5 to 1.0 is observed by altering the upper and lower bounds of $\xi$. In trial calculation optimization, the algorithm's initial trial runs with various $\xi$ profiles can assist in finding a configuration that strikes a balance between global search capacity and convergence speed. It is frequently discovered that linear decay between 1.0 and 0.5 offers a strong trade-off between exploration and exploitation, preventing premature convergence while yet permitting fine-tuning close to the global optimum.

**Algorithm 1:** QPSO optimization procedure

**Input:** Population size $P$, Dimension $D$, and MG system parameters.
**Initialization:** Create a random initial population according to the MG configuration. Analyze the current position $x_{p,q}$, personal best $P_{p,q}$ and global best $G_q$.
**While** $(iter_{count} < iter_{max})$ **do**
    Set $t = t + 1$
    Calculate the mean optimal position:
    $mbest_{p,q}(t) = \frac{1}{Gm}\sum_{p=1}^{Gm} P_{p,q}(t)$
    Choose a suitable contraction-expansion $\xi$ value:
      $\xi = 1 - (1 - 0.5) * k/Gm$
      **For** each particle $p = 1\ to\ M$ **do**
      **For** each dimension $q = 1\ to\ N$ **do**
        Create a random number $\varphi \in [0,\ 1]$
        Update:
        $P_{p,q}(t) = \left(\varphi * P_{p,q}(t) + (1 - \varphi) * G_q(t)\right)$
        Create a random number $u \in [0,\ 1]$
        **If** $\varphi > 0.5$
        $x_{p,q}(t+1) = P_{p,q}(t) - \xi * \left|mbest_{p,q}(t) - x_{p,q}(t)\right| * In\left(\frac{1}{u}\right)$
        **Else**
        $x_{p,q}(t+1) = P_{p,q}(t) + \xi * \left|mbest_{p,q}(t) - x_{p,q}(t)\right| * In\left(\frac{1}{u}\right)$
        **End if**
        **End for**
        Evaluate the objective function of $x_{p,q}(t+1)$ and calculate the MG total operating cos t $F(\chi)$.
        Update $P_{p,q}(t)$ and $G_q$.
      **End for**
    **End all**

The Table 1 displays the selection of the social acceleration coefficient ($c_1$), cognitive acceleration coefficient ($c_2$) and contraction–expansion coefficient $\xi$ as discussed in Ref. [35], it is important to take the following points into consideration.

1. If $c_1 > c_2$ particles attract more towards their own personal best position, resulting in too much scattering particles.
2. Conversely, $c_2 > c_1$ particles attract more towards the global best position and rush prematurely towards the optimal position.
3. On the other hand, if $c_1 = c_2$, particles attract towards the average position.

**Table 1.** Optimization parameter values.

| Parameter | Values |
| --- | --- |
| Number of particles $(N)$ | 50 |
| Maximum number of iterations $(iter_{max})$ | 200 |
| Contraction–expansion coefficient $(\xi)$ | 0.5 |
| Social acceleration coefficient $(c_1)$, | 1.5 |
| Cognitive acceleration coefficient $(c_2)$ | 2.0 |

The chosen QPSO parameters in this study have a direct impact on the quality of the solution and the rate of convergence. A swarm size of 50 particles offers a fair compromise between computational cost and search diversity, allowing sufficient exploration of the solution space without requiring an excessive amount of runtime. While avoiding pointless calculations, the maximum iteration limit of 200 guarantees enough time for convergence toward the global optimum. By progressively decreasing particle spread, the contraction–expansion coefficient ($\xi$ = 0.5) encourages convergence stability. The social ($c_1$ = 1.5) and cognitive ($c_2$ = 2.0) acceleration coefficients encourage particles to effectively converge toward high-quality solutions while preventing premature convergence by striking a balance between individual learning and global guiding.

## 5. Implementation of QPSO Framework

This section examines how the proposed algorithm is implemented to optimize energy scheduling and examines how the DSM program affects a typical MG. However, before implementing the proposed optimization framework, bid costs are calculated for each DG unit with maximum and minimum power limits. All of the power sources in the MG have their maximum and minimum power outputs listed in Table 2. These outline each distributed generation (DG) unit's operating parameters, including its minimum and maximum power capacity, inside the microgrid. The optimization algorithm is guided by these limitations to schedule power generation and storage within safe and effective operating ranges while preserving system dependability and balance. Furthermore, the key environmental and economic factors for each DG source in the MG are listed in Table 3. Emission parameters for $CO_2$, $SO_2$, and $NO_x$ that evaluate environmental impact are included, as are bid and start-up/shut-down costs that affect economic dispatch. Emissions from fossil fuel units like MT and FC are higher than those from renewable sources like PV and WT. When scheduling microgrid energy, these characteristics help the optimization model strike a balance between environmental sustainability and cost effectiveness. The bid price of 0.380 €/kWh represents the discharging (selling) cost of the Battery Energy Storage System (BESS), corresponding to the price at which stored energy is supplied to the grid or local loads. To enhance model realism, the charging (buying) cost is differentiated and set lower at 0.300 €/kWh, reflecting the cost of purchasing energy from the grid. In addition, a nonlinear aging cost that increases with depth of discharge is incorporated to capture battery degradation effects. Figure 6 illustrates the BESS aging cost characteristics as functions of depth of discharge and state of charge.

The flowchart of the proposed optimization framework is shown in Figure 7. There are three phases in the proposed structure. This framework's scenario-generating module is the first step. It uses the probability distribution function (PDF) to assess PV and WT power production by assigning a random variable with a range of [0, 1]. The second element of the framework receives the best feasible scenarios produced in the module as input, along with DG bid prices, load forecasts, MG operational parameters, and limitations. The second step examined how the target function of the scheduling problem, load predictions for various levels of DSM participation, and the constraints placed on each power source affected the MG's ability to access the carbon trading market. The final step involves building an optimization using the QPSO method. The effects of different DSM involvement levels on MG's economy and operational stability are investigated, and various load prediction profiles and other variables are used as inputs to optimal models. The proposed QPSO optimization framework estimates the power exchange between the utility, DGs, and energy storage, and looks at the output cost of each energy source to reduce the operational cost, which is subject to the intricate limitations of the MG.

**Table 2.** Energy sources: minimum and maximum output [48].

| Unit | Type | Min Power (kWh) | Max Power (kWh) |
|---|---|---|---|
| 1 | MT | 6 | 30 |
| 2 | FC | 3 | 30 |
| 3 | PV | 0 | 25 |
| 4 | WT | 0 | 15 |
| 5 | BESS | −30 | 30 |
| 6 | Utility | −30 | 30 |

**Table 3.** Bids and emissions of the DG sources [48].

| Unit | Type | Bid (€/kWh) | Start-Up/Shut-Down Cost (€) | $CO_2$ (kg/MWh) | $SO_2$ (kg/MWh) | $NO_x$ (kg/MWh) |
|---|---|---|---|---|---|---|
| 1 | MT | 0.457 | 0.96 | 720 | 0.004 | 0.100 |
| 2 | FC | 0.294 | 1.65 | 460 | 0.003 | 0.008 |
| 3 | PV | 2.584 | 0.00 | 0 | 0.000 | 0.000 |
| 4 | WT | 1.073 | 0.00 | 0 | 0.000 | 0.000 |
| 5 | BESS | 0.380 | 0.00 | 10 | 0.002 | 0.001 |

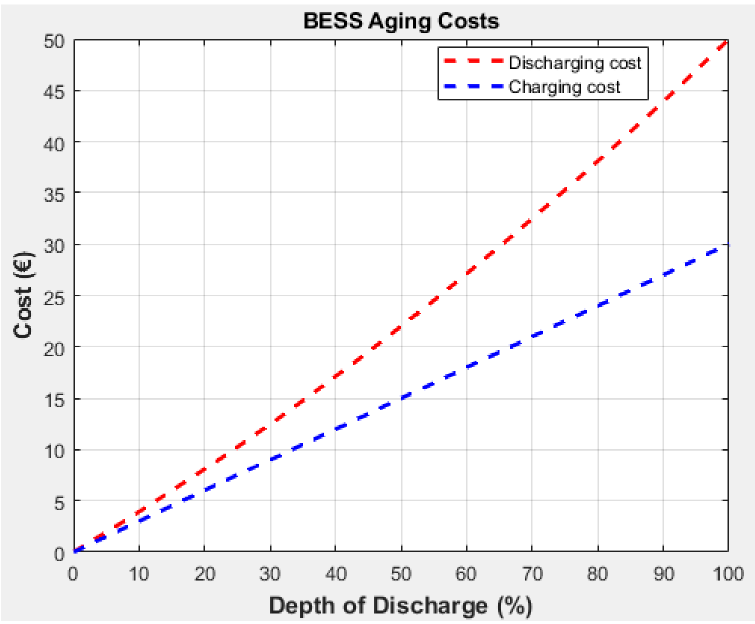


**Figure 6.** Efficiency costs of BESS model.

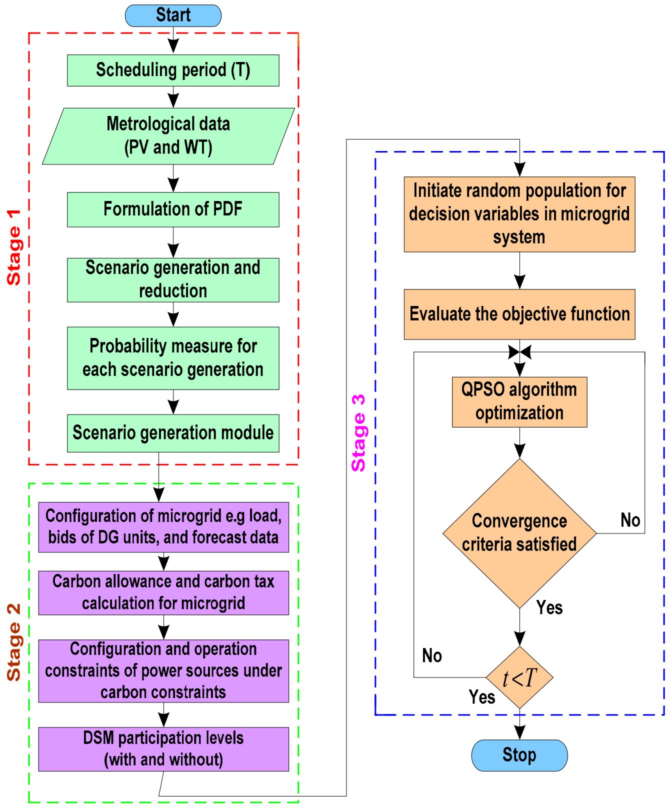


**Figure 7.** Proposed flowchart of the QPSO framework.

*Simulation Evaluation Criteria*

Similar to those in Ref. [38], a thorough case study is carried out to confirm the effectiveness and computational efficiency of the proposed QPSO-based multi-factor resource allocation system using real-time meteorological data from a residential microgrid situated in Oud-Heverlee, North-East Belgium. The selected MG consists of 10 distributed energy nodes, including 15 photovoltaic (PV) generation units, 10 wind turbines, and 10 energy storage systems (ESSs). The MG runs on the main grid and has a backup energy storage system with a total installed capacity of 6 MWh. Its 600-kWh battery module has a depth-of-discharge (DoD) limit of 85% to guarantee battery longevity. The maximum charge/discharge cycle for each storage unit is twice daily, and the round-trip efficiency of the units is set at 92%. The total installed PV capacity is 35 kW, of which 30 kW is generated by wind under ideal wind speed conditions. Furthermore, the case study covers a one-year operational horizon, divided into four seasonal scenarios to capture the impact of seasonal variations on renewable generation and demand-side behavior. The demand-side data is based on past patterns of home power consumption, with summer demand peaking at 3.8 kW and winter demand being comparatively lower at 2.6 kW. The standard MG presented in Figure 2, which consists of BESS, FC, WT, PV, and MT, has been used to study this case. By connecting the MG to the utility grid, the Point of Common Connection (PCC) enables power exchange when needed. Accordingly, the demand-side load participation percentages are 10%, 20%, 30%, and 40%. The microgrid's integration of 50 demand response (DR) participants, who modify their energy usage in response to dynamic pricing signals, makes a total of 1695 kWh of flexible load accessible during peak demand periods. One hour is the unit time interval, while one day (24 h) is the dispatching time. A 5% contingency reserve requirement is implemented to account for practical limitations and preserve system stability in the event of unforeseen changes in supply or demand.

For result analysis and visualization, the MATLAB R2021b version 9.10.0.1577079 software is used to implement the proposed QPSO technique, and a Dell Core i5-latitude E7270 CPU operating at 2.50 GHz and 8 GB of RAM were used for the experimental simulation. The TensorFlow and Scipy optimization libraries are used in the parameter adjustment steps. Near real-time optimization is made feasible by limiting the computation duration per scheduling instance to 10 min. The swarm size is represented by the number of particles $(N)$, and the maximum number of iterations $(iter_{max})$ is set at 50 and 200, respectively, to provide ample opportunity for convergence. The acceleration coefficients $(c_1, c_2)$ are set to 1.5 and 2.0. In contrast, the contraction-expansion coefficient $(\xi)$ which is crucial in regulating the particle search behavior, is set at 0.5. The suggested case study provides a realistic testbed for evaluating the practicality of QPSO in microgrid scheduling by contrasting its performance with state-of-the-art dispatching strategy techniques such as Adaptive Multiple Particle Swarm Optimization (AMPSO) [38], Real-Coded Genetic method (RCGA) [49], and Tent Map Differential Evolution (TMDE) [50]. The output of every RES, as well as the communication between the utility grid and the MG, was acquired for this study. For the TMDE approach, the scaling factor $(k)$ is set at 0.5, and the crossover probability $(p_C)$ is set at 0.7. For RCGA, both the crossover and mutation distribution indices are assumed to be 4, and the corresponding probabilities are assumed to be 0.8 and 0.2. The maximum inertia weight of AMPSO is 0.89, while the minimum inertia weight is 0.41. The cognitive and social qualities are taken to be 2 and 2, respectively. Similar to QPSO, the number of iterations and population size of TMDE, RCGA, and AMPSO are considered as 50 and 200, respectively.

## 6. Results and Discussion

Five (5) assumptions were considered for the simulation experiments in this section: (1) All of the network's loads are electrical, and no heating load is taken into account (2) The optimization system gives WT and PV power generation priority to maximize RESs consumption (3) In the MG network, the power output at the PCC is at unity power factor (4) In grid-connected MG, the dynamics of the loads are not considered (5) With its huge capacity, the BESS can supply power for many hours. To assess the proposed framework, five (5) case studies are taken into consideration based on these assumptions. Case 1, which is regarded as the base case, uses a QPSO optimizer to solve the MG scheduling problem with the aim of minimizing total operating costs. This base case analyzes the operating cost effects of utility and DG units' power exchange in the absence of the load demand. Accordingly, the demand-side load participation percentages of 10%, 20%, 30%, and 40% are set for Cases 2 to 5, respectively.

### *6.1. Case 1: Base Case Without DSM Implementation*

In Case 1, power exchange between the residential load and the microgrid is managed by the MGCC, while MT, FC, and BESS units are given priority during the scheduling process. Scheduling power profiles for DG units and the exchange's power without load demand are shown in Figure 8. The FC supplies a significant amount of the energy because its bids are lower than those of the other units throughout the analyzed time. As market prices rise between 9 h and 17 h and 21 h and 22 h, more MT is produced, and excess energy is exported from the MG to the utility. In order to improve MG resilience for each DG source, the dispatch solution prioritizes BESS utilization during the time of high energy prices, which is from 8 h to 18 h, and minimizes MG–utility power exchange between 20 h and 22 h. However, for the backup option, PV and WT are saved. The output characteristics of WT and PV differ, which contribute to the MG during peak demand from 9 h to 16 h, increasing energy exports to the utility. The contribution of renewable power output decreases because of the high bid prices for other DG units. Simulations showed that utilizing RESs produces better and more cost-effective results. The unpredictability of RES power generation, however, makes it unsuitable. Figure 9 shows the RESs' scheduling cost profile, which aims to reduce overall operating costs. MG's generating units have an overall operating cost of 267.10 €. In Table 4, the base-case simulation result is presented, and the MG's operating cost is compared with other optimization results. The results show that the suggested QPSO algorithm performs better than the compared optimization techniques in terms of computational efficiency and solution quality. In particular, QPSO had the lowest operating cost of 267.10 €, which is an improvement of 0.99% over AMPSO, 10.52% over RCGA, and 20.04% over TMDE. Additionally, QPSO had the fastest computation time (6.21 s), demonstrating its superior convergence speed and lower computational load. In comparison to RCGA, TMDE, and AMPSO, respectively, the suggested QPSO exhibits a stronger balance between exploration and exploitation, allowing it to produce higher-quality solutions in less computing time.

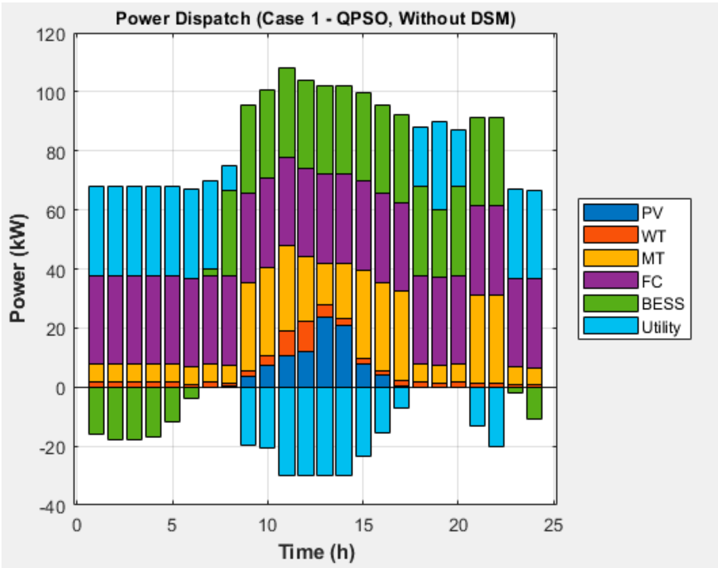


**Figure 8.** Schedule power profile of PV, WT, FC BESS, and Utility without DSM.

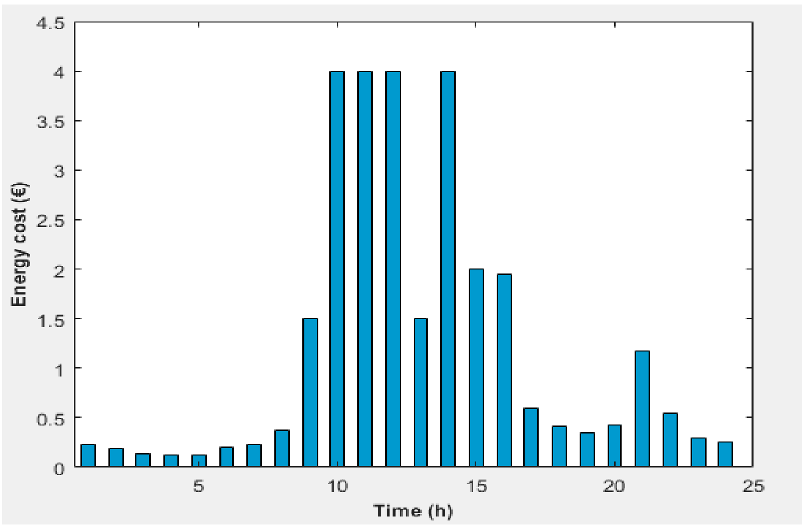


**Figure 9.** Schedule cost profile of RESs.

**Table 4.** Simulated test results for Case 1, only economic scheduling.

| Algorithm | Operating Cost (€) | Computation Time (s) |
|---|---|---|
| RCGA [49] | 298.51 | 10.32 |
| TMDE [50] | 334.03 | 12.45 |
| AMPSO [38] | 269.76 | 8.76 |
| Proposed QPSO | 267.10 | 6.21 |

### *6.2. Case 2: Implementation of DSM with 10% Load Participation*

Case 2 examines the impact of DSM with 10% load participation on the microgrid. The economic power dispatch of DG sources using the QPSO optimizer is shown in Figure 10. The simulation's outcome clearly shows that, in comparison to Case 1, the overall operating cost decreases. In the same way, the output power of FC reaches its highest value throughout the day; FC supplies a major portion of the energy while the MT reaches its minimum during times when market prices are low and its maximum during times when market prices are high. During periods of low utility market rates, the BESS is set to charge between 5 h and 7 h and between 23 h and 24 h. During peak hours, the battery uses its stored energy to power the load and exports the remaining energy to the grid. The power output regulations governing the WT and PV RESs are different. During peak demand, which occurs between 9 h and 14 h, it is noticed that PV and WT contribute to MG, increasing the amount of energy exported to the utility. Thus, because PV and WT bid prices are high compared to other DG units, the contribution of renewable power output steadily rises and falls. The MG's generating units have an overall operating cost of 155.01 €. The percentage decrease in MG operation costs is 41.97% as compared to Case 1, which does not take DSM participation into account.

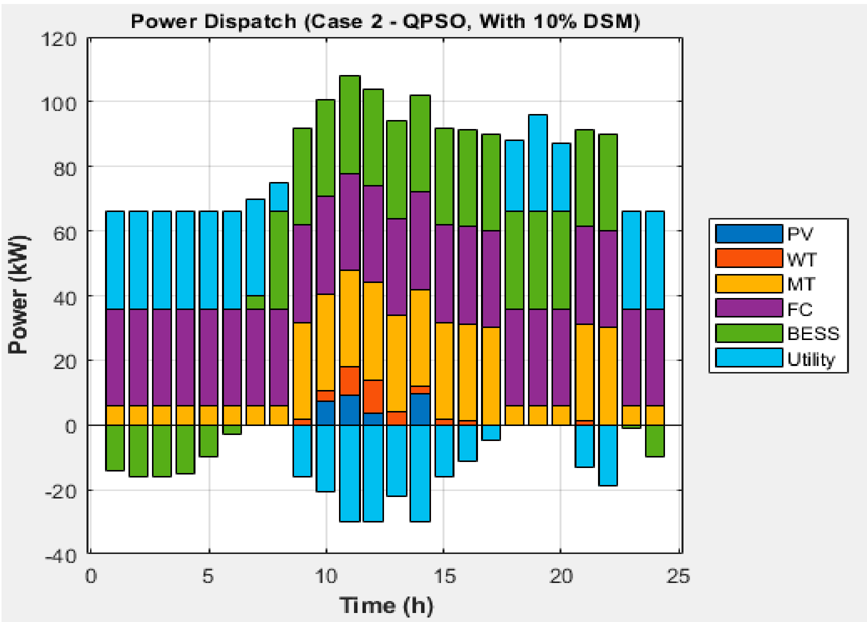


**Figure 10.** Schedule power profile of PV, WT, FC BESS, and Utility with 10% DSM.

### 6.3. Case 3: Implementation of DSM with 20% Load Participation

In Figure 11, the scheduling power profile of MGs with a deployment of 20% load participation of DSM is presented. During the scheduling process, MT, FC, and BESS units are prioritized. Due to its lowest bid price as compared to other DG units, the data gathered shows that the utility is used up to 127 kW through the PCC. The MT energy consumption is regulated to its minimum limit of 6 kW for the first 1 to 6 h and 18 to 21 h since it exceeds the utility market price. From an economic perspective, PV and WT activate when the MG's internal power output is insufficient or when additional energy must be exported to the grid. Additionally, PV and WT modify their generating set-points based on the amount of load at each hour of the day. The MG's generating units have an overall operating cost of 68.18 €. When DSM involvement is not considered, the percentage decrease in MG operation costs is 74.48% when compared to case 1. In contrast, Case 2 yields a 56.02% reduction in MG operation costs when DSM involvement is considered.

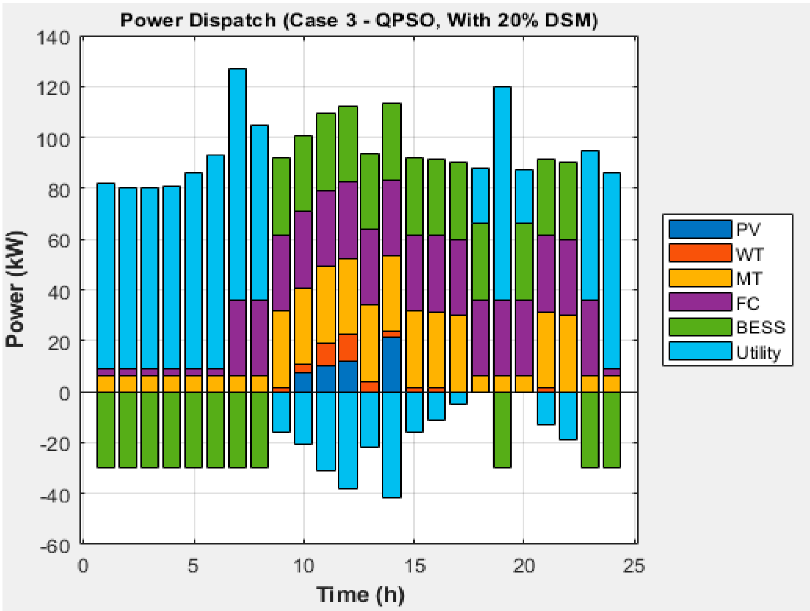


**Figure 11.** Schedule power profile of PV, WT, FC BESS, and Utility with 20% DSM.

### 6.4. Case 4: Implementation of DSM with 30% Load Participation

Figure 12 shows the scheduling power profile of MGs with a deployment of 30% load participation of DSM. Due to the higher bids of corresponding units compared to other units during the examined period, the FC and MT within the utility supply a significant portion of the energy during the first hour of the day. As with case 3, it is found that the overall BESS usage is further optimized, and the charging process is completed between 16 h and 17 h of the day when prices are low. However, the discharge action is delayed to the first hour of the day, between 6 h and 7 h, when the generation of RESs is lower. Alternatively, WT and PV modify their generating set-points based on hourly load levels. In Case 4, the efficient scheduling of all DG units lowers MG power imports during periods of high demand and substantially increases total energy exports. MG's generating units have an overall operating cost of 44.23 €. The percentage decrease in MG operation costs is 83.44% as compared to Case 1, which does not take DSM involvement into account. When DSM participation is considered, the percentage reduction in MG operation expenses is 71.47% in case 2 and 35.13% in case 3.

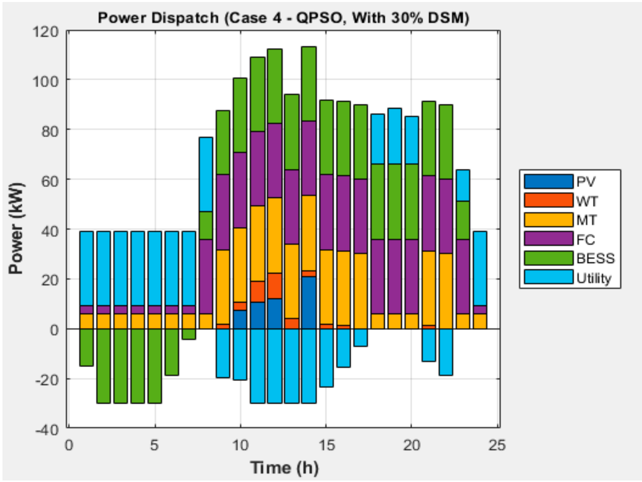


**Figure 12.** Schedule power profile of PV, WT, FC BESS, and Utility with 30% DSM.

*6.5. Case 5: Implementation of DSM with 40% Load Participation*

Figure 13 illustrates the optimal economic power dispatch while employing QPSO to schedule the DG units for the next day with a 40% DSM load participation level. Compared to previous cases, the results indicate that the scheduled electricity from all DG units is modified so that the MG boosts overall export energy and purchases less power from the utility during peak demand. From an economic standpoint, WT and PV are sent out when the grid experiences power outages or more energy export to the macro-grid is needed. To guarantee economical operation, FC, MT, and BESS also modify their generation set-points on an hourly basis based on load levels. MG's generating units have an overall operating cost of 22.68 €.

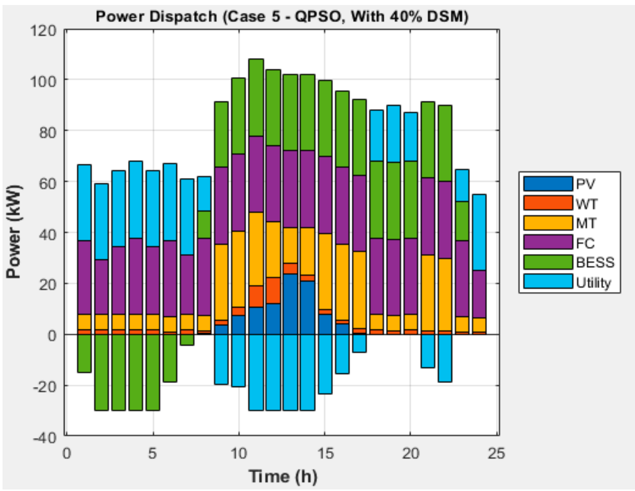


**Figure 13.** Schedule power profile of PV, WT, FC BESS, and Utility with 40% DSM.

The MG percentage operational cost is 91.54% lower than in Case 1 (without DSM participation). The percentage decreases for Cases 2, 3, and 4 with DSM participation are 48.90%, 66.85%, and 85.42%, respectively. The obtained result shows that the MG operational cost dramatically decreases as the DSM participation level increases. The MG operating expenses with and without DSM involvement levels are contrasted in Table 5. The installation of the DSM program shifts controlled loads to off-peak hours, giving the load pattern flexibility to fit the generation profile. Table 6 displays the MG operator's daily energy cost savings for different DSM engagement levels depending on the outcomes attained. We conclude from the analysis that the MG operator can lower daily operating expenses and perhaps increase yearly financial savings.

**Table 5.** Simulated results of MG operating expenses.

| Case ID | Operating Cost (€) | Computation Time (s) | DSM Participation |
|---|---|---|---|
| Case 1 | 267.10 | 12.45 | x |
| Case 2 | 155.01 | 10.3 | 10% |
| Case 3 | 68.18 | 8.7 | 20% |
| Case 4 | 44.23 | 7.5 | 30% |
| Case 5 | 22.68 | 6.2 | 40% |

**Table 6.** Daily energy cost savings.

| DSM Level | Reduction Cost (%) | | | |
|---|---|---|---|---|
| | Scenario 1 | Scenario 2 | Scenario 3 | Scenario 4 |
| 10% | 41.97 | - | - | - |
| 20% | 74.48 | 56.02 | - | - |
| 30% | 83.44 | 71.47 | 35.13 | - |
| 40% | 91.54 | 85.42 | 66.85 | 48.90 |

### *6.6. Scheduling of DG Sources Under Carbon Emission*

The only traditional power sources in the proposed MG that use natural gas or biogas are microturbines (MT) and fuel cells (FC). When compared to other DG units, these emit a lot more carbon dioxide ($CO_2$) per kilowatt-hour of generation. This study focuses on employing the QPSO optimizer to dispatch MT and FC under carbon emission without DSM load participation. The optimal scheduling results for each emission dispatch are shown in Figure 14. At 1 h, 3 h, 7 h, and 9 h, respectively, the MT output is higher. The MT's power production will be raised to charge the BESS during the 2 h, 6 h, and 14 h periods, which correspond to the off-peak demand period, regarding the carbon trading market. Likewise, the same logic applies to FC as well. By increasing MT's power output, the cost of electricity purchased drops between 15 h and 17 h. The overall carbon emission is optimized to 797.110 kg once the carbon trading market is implemented. The validation simulation result is presented in Table 7. The compared findings unequivocally show that the suggested QPSO algorithm provides superior performance in terms of convergence speed and solution quality. In particular, QPSO produces the least amount of carbon emissions (797.11 kg), which is 7.074% less than AMPSO, 8.077% less than RCGA, and 8.894% less than TMDE. Furthermore, QPSO produces lower-emission solutions more effectively than RCGA, TMDE, and AMPSO because of its quantum-inspired search mechanism, which improves global exploration and convergence stability. QPSO converges in just 6.21 s. Additionally, a pairwise t-test between the suggested QPSO and the comparison algorithms was conducted to guarantee the stability of the acquired emission values. The statistical significance of the emission decrease attained by QPSO is confirmed by the p-values for every comparison being less than 0.05. This shows that QPSO's better global search capabilities, rather than random stochastic variation, are responsible for its improved performance.

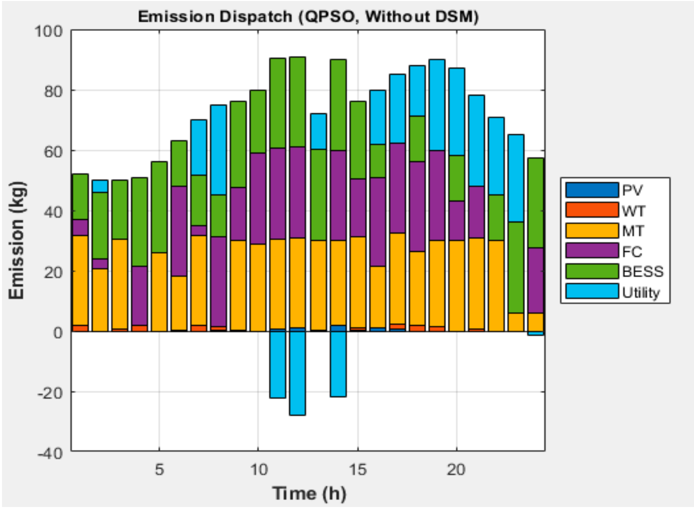


**Figure 14.** Schedule emission profile of PV, WT, FC BESS, and Utility without DSM.

**Table 7.** Simulated test results for Case 1, only emission scheduling.

| Algorithm | Carbon Emission (kg) | Computation Time (s) |
|---|---|---|
| RCGA [48] | 867.15 | 10.32 |
| TMDE [49] | 874.93 | 12.45 |
| AMPSO [38] | 857.79 | 8.76 |
| Proposed QPSO | 797.11 | 6.21 |

### *6.7. Convergence Characteristics*

Figure 15 shows the convergence validation of TMDE, RCGA, AMPSO, and QPSO for carbon emissions. In the early stages, QPSO is shown to have the lowest volatility, followed by AMQPSO, RCGA, and TMDE. The proposed QPSO converges before 150 iterations, AMPSO stabilizes before 160 iterations, while RCGA achieves stability after 180 iterations. In contrast, TMDE continues searching and does not converge until 200 iterations. TMDE, RCGA, AMPSO, and QPSO have total emission values of 874.93 kg, 867.15 kg, 857.79 kg, and 797.11 kg, respectively. As a result, the QPSO is more sensitive and efficient in ensuring the system runs both economically and environmentally. Additionally, Figure 16 depicts the impact of carbon emissions and the cost of MG operations. The outcome is contrasted with the outcomes of other optimization experiments. The results show that QPSO has lower carbon emissions and lower operating costs than other optimizations for solving the MG scheduling problem identified in this study. According to the scenario, it is found that a greater integration of RESs into the grid environment leads to decreased emissions, but at the expense of increased operating costs. On the other hand, RESs have lower operating costs and produce higher emissions when they are less widely integrated into the grid. The computational complexity of the proposed QPSO algorithm increases with microgrid size, number of distributed energy resources (DERs), and the length of the scheduling horizon. As the number of DERs grows, the dimensionality of the decision vector expands linearly, leading to higher per-iteration evaluation costs. Similarly, longer scheduling horizons increase the number of time-indexed variables, resulting in a proportional rise in fitness function computations.

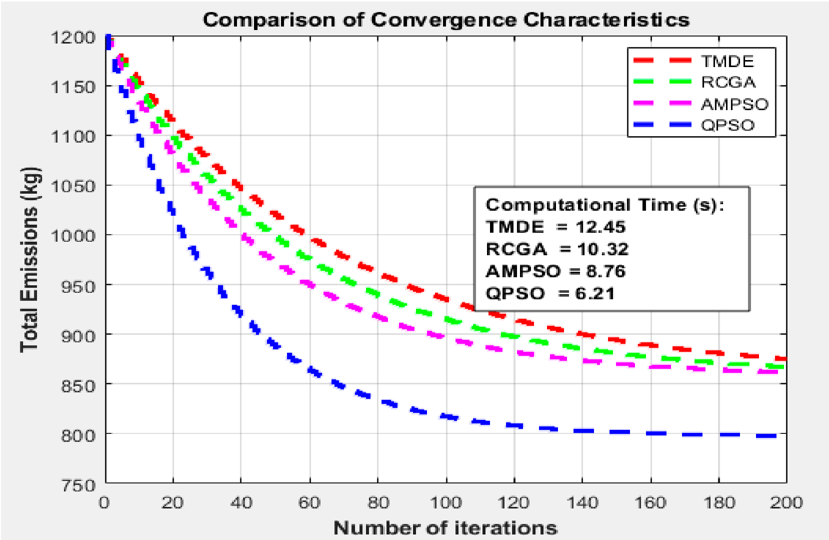


**Figure 15.** Comparison of emission convergence characteristics.

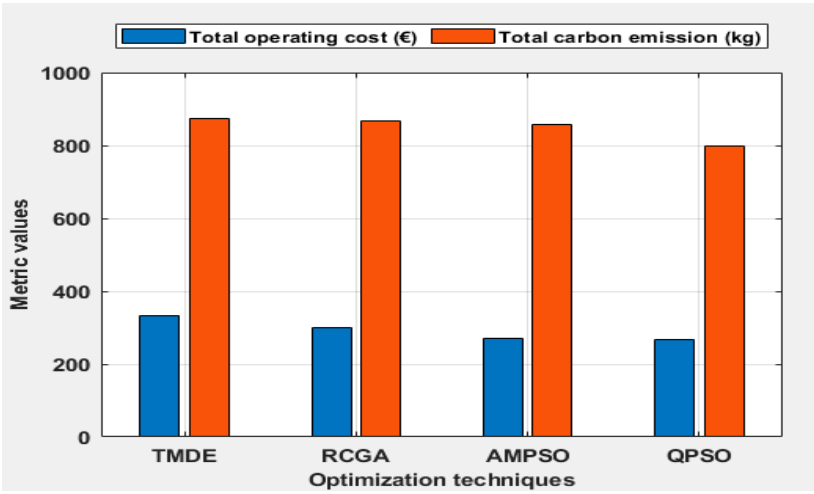


**Figure 16.** Comparison of emission and cost schedule profile.

*6.8. Estimation of Greenhouse Gas (GHG) Emission*

Table 8 illustrates the GHG emissions from each DG source, which were computed according to their individual ratings. During operation, the PV and WT did not emit any GHG. It has very little life-cycle impact and emits very little GHG. Every year, the FC uses natural gas to generate about 136,159.563 kg of GHG emissions. On the other hand, the natural gas-powered MT emits roughly 154,798.201 kg of GHG annually. As a result of using natural gas, the gas-fired MT produces the most GHG. When a thermal power plant uses coal to generate the same amount of energy from DG sources, it releases 555,667.695 kg of GHG emissions. This discrepancy is further demonstrated by the annual GHG emissions: the coal-fired thermal power plant emits 555,668 kg/year, whereas the total emissions from all DG sources are only 290,958 kg/year. By showing how low-carbon DG technologies can lower the overall carbon footprint of power generation when compared to conventional fossil-fuel-based plants, this comparison highlights the environmental rationale and benefit of including them in microgrid systems. The GHG emissions of the modeled MG were reduced by about 48% as compared to its coal-powered counterpart.

**Table 8.** Estimated GHG emissions for the DG sources.

| DG Sources | Rating (kW) | GHG Emission (kg/kWh) | Energy Generated (Units/Year) | Total GHG per Year (kg) |
|---|---|---|---|---|
| Solar PV | 35 | 0 | 33,388.375 | 0 |
| WT | 30 | 0 | 20,861.21 | 0 |
| FC | 35 | 0.59 | 230,778.92 | 136,159.563 |
| MT | 40 | 0.63 | 245,711.43 | 154,798.201 |
| Total GHG emission year | | | | 290,957.764 |
| Coal-fired power plant [51] | 100 | 1.98 | 280,640.25 | 555,667.695 |

## 7. Conclusions

This paper illustrates how to tackle MG scheduling issues under utility-induced DSM programs using stochastic analysis and large multi-objective QPSO. Furthermore, this work suggests a three-phase scenario to address the uncertainties related to RESs while utilizing DSM to resolve the energy scheduling problem over 24 h. Five (5) case studies in all were analyzed with real-time weather data. Four percentages of load participation—10%, 20%, 30%, and 40%—were employed to evaluate DSM's impact on the MG. Out of all the case studies, the best optimization result is achieved at a higher DSM participation level of 40%. Cost reductions of 91.54%, 85.42%, 66.85%, and 48.90% are achieved when comparing this scenario to others. This study concludes, based on simulation results, that the QPSO approach significantly lowers costs, minimizes environmental impacts, improves reliability in the face of fluctuating energy demands, and supports more sustainable energy practices. The suggested QPSO-based optimization methodology is appropriate for larger and more intricate microgrid systems because of its great scalability and adaptability. Because of its quantum-behaved mechanism, which successfully strikes a balance between local exploitation and global exploration, QPSO maintains great computational efficiency as system complexity rises. In addition, it provides significant improvements in energy distribution optimization and peak load demand management, and it successfully resolves the MG scheduling issue.

## 8. Future Recommendation

With the development of quantum-inspired technologies, the energy industry stands to gain new insights into the management and optimization of energy systems in a world that is becoming more digital and linked. Future research should concentrate on investigating bigger microgrid systems, integrating more intricate restrictions like cybersecurity and sophisticated predictive analytics, and further improving the quantum algorithms' scalability and efficiency. Furthermore, it's worthwhile to look into how advanced analytics techniques like deep learning and AI-driven optimization might improve energy scheduling, power generation forecasts, and energy management models. These strategies improve forecast accuracy and assist MG's operators in making optimal energy scheduling decisions by making it possible to extract complex patterns from complex energy data. Furthermore, future studies could expand the suggested framework to take into consideration real-world uncertainties such as communication delays, demand variations, and inaccuracies in renewable predictions. The resilience and dependability of the model for real-time microgrid operation and large-scale smart grid applications will be further improved by using stochastic or scenario-based optimization together with adaptive control methods.

**Author Contributions:** Conceptualization, K.E.O., A.K.S. and V.M.S.; methodology, K.E.O.; A.K.S. and V.M.S.; software, K.E.O.; validation, K.E.O., A.K.S. and V.M.S.; formal analysis, K.E.O.; investigation, K.E.O.; resources, K.E.O.; data curation, K.E.O.; writing—original draft preparation, K.E.O.; writing—review and editing, A.K.S. and V.M.S.; visualization, A.K.S. and V.M.S.; supervision, A.K.S. and V.M.S.; project administration, A.K.S. and V.M.S. All authors have read and agreed to the published version of the manuscript.

**Funding:** This research received no external funding.

**Data Availability Statement:** The dataset that supports the findings of this study is openly available and published by Moghaddam et al. [38] under the Creative Commons Attribution (CC BY 4.0) license, while the modified dataset is available from the authors upon request.

**Conflicts of Interest:** The authors declare no conflicts of interest.

## References

1. Ishraque, M.F.; Rahman, A.; Shezan, S.A.; Shafiullah, G.M.; Alenezi, A.H.; Hossen, M.D.; Bintu, N.E.N. Design Optimization of a Grid-Tied Hybrid System for a Department at a University with a Dispatch Strategy-Based Assessment. *Sustainability* **2024**, *16*, 2642. [CrossRef]
2. U.S. Department of Energy. *Microgrid Overview: Grid Deployment Office Fact Sheet*; DOE Grid Deployment Office: Washington, DC, USA, 2024; pp. 1–9.
3. Adegboyega, A.W.; Sepasi, S.; Howlader, H.O.R.; Griswold, B.; Matsuura, M.; Roose, L.R. DC Microgrid Deployments and Challenges: A Comprehensive Review of Academic and Corporate Implementations. *Energies* **2025**, *18*, 1064. [CrossRef]
4. Alluraiah, N.C.; Vijayapriya, P. Optimization, Design and Feasibility Analysis of a Grid-Integrated Hybrid AC/DC Microgrid System for Rural Electrification. *IEEE Access* **2023**, *11*, 67013–67029. [CrossRef]
5. Chakraborty, A.; Ray, S. Economic and Environmental Factors-Based Multi-Objective Approach for Optimizing Energy Management in a Microgrid. *Renew. Energy* **2024**, *222*, 119920. [CrossRef]
6. Ojo, K.E.; Saha, A.K.; Srivastava, V.M. Microgrids' Control Strategies and Real-Time Monitoring Systems: A Comprehensive Review. *Energies* **2025**, *18*, 3576. [CrossRef]
7. Ojo, K.E.; Saha, A.K.; Srivastava, V.M. Review of Advances in Renewable Energy-Based Microgrid Systems: Control Strategies, Emerging Trends, and Future Possibilities. *Energies* **2025**, *18*, 3704. [CrossRef]
8. Khaleel, M.M.; Ahmed, A.A.; Alsharif, A. Energy Management System Strategies in Microgrids: A Review. *N. Afr. J. Sci. Publ.* **2023**, *1*, 1–8.
9. Imran, A. Heuristic-Based Programmable Controller for Efficient Energy Management under Renewable Energy Sources and Energy Storage System in Smart Grid. *IEEE Access* **2020**, *8*, 139587–139608. [CrossRef]
10. Hemmati, M.; Bayati, N.; Ebel, T. Integrated Optimal Energy Management of Multi-Microgrid Network Considering Energy Performance Index: Global Chance-Constrained Programming Framework. *Energies* **2024**, *17*, 4367. [CrossRef]
11. Tajjour, S.; Chandel, S.S. A Comprehensive Review on Sustainable Energy Management Systems for Optimal Operation of Future-Generation Solar Microgrids. *Sustain. Energy Technol. Assess.* **2023**, *58*, 103377. [CrossRef]
12. Dey, B.; Dutta, S.; Garcia Marquez, F.P. Intelligent Demand Side Management for Exhaustive Techno-Economic Analysis of Microgrid System. *Sustainability* **2023**, *15*, 1795. [CrossRef]
13. Barnawi, A.B. Development and Analysis of Optimization Algorithm for Demand-Side Management Considering Optimal Generation Scheduling and Power Flow in Grid-Connected AC/DC Microgrid. *Sustainability* **2023**, *15*, 15671. [CrossRef]
14. Li, J.; Yang, M.; Zhang, Y.; Li, J.; Lu, J. Micro-Grid Day-Ahead Stochastic Optimal Dispatch Considering Multiple Demand Response and Electric Vehicles. *Energies* **2023**, *16*, 3356. [CrossRef]
15. Wang, L. Optimal Scheduling Strategy for Multi-Energy Microgrid Considering Integrated Demand Response. *Energies* **2023**, *16*, 4694. [CrossRef]
16. Roldán-Blay, C.; Miranda, V.; Carvalho, L.; Roldán-Porta, C. Optimal Generation Scheduling with Dynamic Profiles for the Sustainable Development of Electricity Grids. *Sustainability* **2019**, *11*, 7111. [CrossRef]
17. Singh, A.R.; Kumar, R.S.; Bajaj, M.; Khadse, C.B.; Zaitsev, I. Machine Learning-Based Energy Management and Power Forecasting in Grid-Connected Microgrids with Multiple Distributed Energy Sources. *Sci. Rep.* **2024**, *14*, 19207. [CrossRef] [PubMed]
18. Liu, M.; Liao, M.; Zhang, R.; Yuan, X.; Zhu, Z.; Wu, Z. Quantum Computing as a Catalyst for Microgrid Management: Enhancing Decentralized Energy Systems through Innovative Computational Techniques. *Sustainability* **2025**, *17*, 3662. [CrossRef]
19. Zhang, T.; Zhao, W.; He, Q.; Xu, J. Optimization of Microgrid Dispatching by Integrating Photovoltaic Power Generation Forecast. *Sustainability* **2025**, *17*, 648. [CrossRef]

20. Liu, F.; Duan, P. Research on Optimal Scheduling of Microgrid Based on Improved Quantum Particle Swarm Optimization Algorithm. *EAI Endorsed Trans. Energy Web* **2024**, *11*, 1–12. [CrossRef]
21. Mgobhozi, B.; Nleya, B. Quantum PSO-Based Power Demand and Supply Management Algorithm for Microgrids. *Nanotechnol. Percept.* **2024**, *20*, 980–992.
22. Zhao, A.P.; Alhazmi, M.; Huo, D.; Li, W. Psychological Modeling for Community Energy Systems. *Energy Rep.* **2025**, *13*, 2219–2229. [CrossRef]
23. Qiu, H.; Liu, P.; Gu, W.; Zhang, R.; Lu, S.; Gooi, H.B. Incorporating Data-Driven Demand-Price Uncertainty Correlations into Microgrid Optimal Dispatch. *IEEE Trans. Smart Grid* **2024**, *15*, 2804–2818. [CrossRef]
24. Han, T.; Xu, Y. Topology-Based Stabilization of Islanded Microgrids with Multiple Tie Switches under Operational Variations: A Neural Control Approach. *IEEE Trans. Power Syst.* **2024**, *40*, 1802–1815. [CrossRef]
25. Prior, J.; Drees, T.; Miro, M.; Kuhlenkotter, B. Systematic Literature Review of Heuristic-Optimized Microgrids and Energy-Flexible Factories. *Clean Technol.* **2024**, *6*, 1114–1141. [CrossRef]
26. Chen, S.; Liu, J.; Cui, Z.; Chen, Z.; Wang, H.; Xiao, W. A Deep Reinforcement Learning Approach for Microgrid Energy Transmission Dispatching. *Appl. Sci.* **2024**, *14*, 3682. [CrossRef]
27. Ju, X.; Fu, P.; Settegast, R.R.; Morris, J.P. A Coupled Thermo-Hydro-Mechanical Model for Simulating Leakoff-Dominated Hydraulic Fracturing with Application to Geologic Carbon Storage. *Int. J. Greenh. Gas Control* **2021**, *109*, 103379. [CrossRef]
28. Mohan, H.M.; Dash, S.K. Renewable Energy-Based DC Microgrid with Hybrid Energy Management System Supporting Electric Vehicle Charging System. *Systems* **2023**, *11*, 273. [CrossRef]
29. Sharma, S.K.; Kaur, T.; Arora, M.K.; Upadhyay, S. Resource Estimation and Sizing Optimization of PV/Micro Hydro-Based Hybrid Energy System in Rural Area of Western Himalayan Himachal Pradesh in India. *Energy Sources Part A* **2019**, *41*, 2795–2807.
30. Naderi, E.; Asrari, A. A Deep Learning Framework to Identify Remedial Action Schemes against False Data Injection Cyberattacks Targeting Smart Power Systems. *IEEE Trans. Ind. Inform.* **2024**, *20*, 1208–1219. [CrossRef]
31. Li, S.; Zhao, A.P.; Gu, C.; Bu, S.; Chung, E.; Tian, Z.; Li, J.; Cheng, S. Interpretable Deep Reinforcement Learning with Imitative Expert Experience for Smart Charging of Electric Vehicles. *IEEE Trans. Power Syst.* **2024**, *40*, 1228–1240. [CrossRef]
32. Li, Y.; Ding, Y.; He, S.; Hu, F.; Duan, J.; Wen, G.; Geng, H.; Wu, Z.; Gooi, H.B.; Zhao, Y.; et al. Artificial Intelligence-Based Methods for Renewable Power System Operation. *Nat. Rev. Electr. Eng.* **2024**, *1*, 163–179. [CrossRef]
33. Choi, J.; Kim, J. A Tutorial on Quantum Approximate Optimization Algorithm (QAOA): Fundamentals and Applications. In Proceedings of the 2019 International Conference on Information and Communication Technology Convergence (ICTC 2019), Jeju Island, Republic of Korea, 16–18 October 2019; pp. 138–142.
34. Ullah, M.H.; Eskandarpour, R.; Zheng, H.; Khodaei, A. Quantum Computing for Smart Grid Applications. *IET Gener. Transm. Distrib.* **2022**, *16*, 4239–4257. [CrossRef]
35. Goh, H.H.; Shi, S.; Liang, X.; Zhang, D.; Dai, W.; Liu, H.; Wong, S.Y.; Kurniawan, T.A.; Goh, K.C.; Cham, C.L. Optimal Energy Scheduling of Grid-Connected Microgrids with Demand Side Response Considering Uncertainty. *Appl. Energy* **2022**, *327*, 120094. [CrossRef]
36. Paul, K.; Jyothi, B.; Kumar, R.S.; Singh, A.R.; Bajaj, M.; Kumar, B.H.; Zaitsev, I. Optimizing Sustainable Energy Management in Grid-Connected Microgrids Using Quantum Particle Swarm Optimization for Cost and Emission Reduction. *Sci. Rep.* **2025**, *15*, 5843. [CrossRef]
37. Giani, A.; Eldredge, Z. Quantum Computing Opportunities in Renewable Energy. *Comput. Sci.* **2021**, *2*, 393.
38. Moghaddam, A.A.; Seifi, A.; Niknam, T.; Pahlavani, M.R.A. Multi-Objective Operation Management of a Renewable MG (Microgrid) with Back-Up Micro-Turbine/Fuel Cell/Battery Hybrid Power Source. *Energy* **2011**, *36*, 6490–6507. [CrossRef]
39. Liu, H.; Du, W.; Guo, Z. A Multi-Population Evolutionary Algorithm with Single Objective Guide for Many-Objective Optimization. *Inf. Sci.* **2019**, *503*, 39–60. [CrossRef]
40. Radosavljević, J.; Jevtić, M.; Klimenta, D. Energy and operation management of a microgrid using particle swarm optimization. *Eng. Optim.* **2016**, *48*, 811–830. [CrossRef]
41. Fatima, I.; Alqahtani, J.; Habib, R.; Akram, M.; Naz, T.; Alqahtani, A.; Atif, M.; Alyami, S.S. Enhancing grid-connected microgrid power dispatch efficiency through bio-inspired optimization algorithms. *IEEE Access* **2024**, *12*, 23578–23594. [CrossRef]
42. Rangu, S.K.; Lolla, P.R.; Dhenuvakonda, K.R.; Singh, A.R. Recent trends in power management strategies for optimal operation of distributed energy resources in microgrids: A comprehensive review. *Int. J. Energy Res.* **2020**, *44*, 9889–9911. [CrossRef]
43. Kumar, R.S.; Raghav, L.P.; Raju, D.K.; Singh, A.R. Intelligent demand side management for optimal energy scheduling of grid-connected microgrids. *Appl. Energy* **2021**, *285*, 116435. [CrossRef]
44. Radosavljević, J.; Milovanović, M.; Arsić, N.; Jovanović, A.; Perović, B.; Vukašinović, J. Optimal power dispatch in distribution networks with PV generation and battery storage. In Proceedings of the 9th International Conference on Electrical, Electronic and Computing Engineering (IcETRAN 2022), Novi Pazar, Serbia, 6–9 June 2022.
45. Hendy, M.A.; Nayel, M.A.; Abdelrahem, M. Stochastic Demand-Side Management for Residential Off-Grid PV Systems Considering Battery, Fuel Cell, and PEM Electrolyzer Degradation. *Energies* **2025**, *18*, 3395. [CrossRef]

46. Wu, S. A Quantum Particle Swarm Optimization Algorithm Based on Self-Updating Mechanism. In *Research Anthology on Advancements in Quantum Technology*; Information Resources Management Association, Ed.; IGI Global: Hershey, PA, USA, 2021; pp. 1–21.
47. Zhou, N.-R.; Xia, S.-H.; Ma, Y.; Zhang, Y. Quantum Particle Swarm Optimization Algorithm with the Truncated Mean Stabilization Strategy. *J. Algorithms Comput. Technol.* **2022**, *21*, 42. [CrossRef]
48. Alomoush, M.I. Microgrid Dynamic Combined Power–Heat Economic-Emission Dispatch with Deferrable Loads and Price-Based Energy Storage Elements and Power Exchange. *Sustain. Energy Grids Netw.* **2021**, *26*, 100479. [CrossRef]
49. Yang, W.; Peng, Z.; Feng, W.; Menhas, M.I. A Novel Real-Coded Genetic Algorithm for Dynamic Economic Dispatch Integrating Plug-In Electric Vehicles. *Front. Energy Res.* **2021**, *9*, 706–782. [CrossRef]
50. Mandal, S.; Mandal, K.K. Optimal Energy Management of Microgrids under Environmental Constraints Using Chaos Enhanced Differential Evolution. *Renew. Energy Focus* **2020**, *34*, 129–141. [CrossRef]
51. Shirley, J.A.J.; Pooja, R.P.; Reddy, M.J.B. Metaheuristic Algorithm-Based Energy Management System for Electric Vehicle Charging Station. *IEEE Access* **2024**, *12*, 116354–116367. [CrossRef]

**Disclaimer/Publisher's Note:** The statements, opinions and data contained in all publications are solely those of the individual author(s) and contributor(s) and not of MDPI and/or the editor(s). MDPI and/or the editor(s) disclaim responsibility for any injury to people or property resulting from any ideas, methods, instructions or products referred to in the content.